Azimuthal Variations of X-Band Medium Grazing Angle Sea Clutter

Zaynab Guerraou
ONERA, DEMR
FRANCE
zaynab.guerraou@onera.com

Sebastien Angelliaume
ONERA, DEMR
FRANCE
sebastien.angelliaume@onera.com

Charles-Antoine Guerin
Université de Toulon
FRANCE
guerin@univ-tln.fr

Luke Rosenberg
Defence Science and Technology Group
AUSTRALIA
luke.rosenberg@dsto.defence.gov.au

ABSTRACT

The Ingara X-band fully-polarimetric medium grazing angle sea clutter data set was collected in the Australian maritime environment over an angular range of 360° in azimuth and 15° to 45° in grazing. This paper reports further analysis of this data set, focussing on understanding the azimuth variation to enable improved simulation accuracy and extraction of relevant geophysical parameters. This includes some original properties of the co- and cross-polarized normalized radar cross section as a function of the scattering geometry and sea surface parameters. We also assess the performances and limitations of recent sea surface scattering models in the light of this rich data set.

1.0 INRTRODUCTION

The study and modeling of the sea surface clutter in the microwave regime is important for both maritime surveillance (i.e. detecting targets in sea clutter) and for better understanding the maritime environment (i.e. the recovery of geophysical parameters). This latter application has reached a mature state in the last decades with the simultaneous improvements of analytic scattering models [1], descriptions of the sea surface [2–4] and the ever increasing capabilities of airborne and space-borne instruments [5]. In most cases, the sea surface and scattering models provide a satisfactory agreement with the experimental observations, both from the qualitative and quantitative point of view (see [6–10] for the assessment of some recent airborne radar data and [11–13] for spaceborne data). However, some issues remain in understanding and modeling the effects of microwave ocean scattering. These include difficulties in characterising the cross-polarized and horizontally-polarized return, the variability of the normalized radar cross section (NRCS) due to 'forcing' parameters (mixed sea systems, swell, currents, wave age, etc.), the influence of breaking waves, the directional wave number spectrum of short-waves, and azimuthal variations including directional asymmetry. In this paper, we will investigate this final issue using the Ingara X-band medium grazing angles (MGA) sea clutter data set which was collected by the Defence Science and Technology Group [14]. This data set is described in Section 2 with an original technique presented in Section 3 for processing data with weak signal (i.e. clutter) to noise ratios (SNR).

Numerous data sets described in the literature show evidence of azimuthal variation of the NRCS at MGAs with different empirical relationships derived to relate the angular variations to the wind and/or wave directions [15–17].

Rather than propose a new geophysical 'model function' for sea clutter returns, this work is concerned with the characterization of the azimuthal variations and directional asymmetries observed in sea-clutter. The results inferred from this study should eventually be confirmed on other datasets, with the long term objective

being to incorporate them into a physical model. Such an improved model would be useful in estimating the main geophysical parameters such as wind speed and direction, significant wave height and wave age.

In Section 4, we investigate the azimuthal variations of the NRCS for both the horizontal (H) and vertical (V) channels. A vanishing of the secondary downwind maximum is observed with the HH polarization at the lowest grazing angle (15°), thereby confirming the phenomenon observed and modelled in the empirical Georgia Institute of Technology (GIT) mean backscatter model [18]. The directional asymmetries are shown to be polarization-dependent and follow non-monotonic variations with respect to the grazing angle.

In Section 5, the relationships between the different polarization channels are investigated in terms of the underlying physical scattering mechanisms. Section 6 then shows a comparison of the angular variations of the fully-polarized data set with recent scattering and directional sea spectrum models. We show that the agreement with data can be improved by resorting to these recent sea surface scattering models, although there remains a number of observed features which are not correctly modeled.

2.0 The Ingara MGA sea clutter data set

Ingara is a fully-polarimetric X-band radar system maintained within the DST Group in Australia [19]. During the MGA sea-clutter trials, the central frequency was set to 10.1 GHz and the radar collected real aperture I/Q data with range and azimuth resolutions of 0.75 m and 63 m respectively. As shown in Fig. 1, data were collected over a range of sea conditions using a circular spotlight collection with grazing angles spanning 15° to 45°. The total collection across all grazing angles for a single run took approximately 90 minutes and it is not unreasonable to assume that the ocean surface conditions remain relatively unchanged. The MGA sea clutter trials were conducted over several days in two distinct maritime regions. The first 'sea cutter trial' (SCT04) occurred in 2004 over the Southern Ocean, approximately 100 km south of Port Lincoln, South Australia. Eight days of data were collected with environmental conditions summarised in Table 1 (runs 1-8). A further four days of data were collected during the second 'maritime surveillance trial' (MAST06) (runs 9-12). This trial was conducted in 2006 over littoral and open ocean environments near Darwin in the Northern Territory. The sea conditions were measured using DST Group's Tri-axys wave buoy which was located within 50 km of the imaging site. Wind data from several different sources were collected and compared during the trials. For the SCT04, the most reliable wind data were obtained from the Bureau of Meteorology (BoM) automatic weather station located on a cliff top about 50 km north-east of the wave buoy deployment site. Hence it will be subject to some error and possibly some time delay compared to the actual conditions at the wave buoy site. For MAST06, the most reliable wind data were made with a hand-held anemometer on a boat near the imaging area except for one collection where the wind vector predicted by the Australian BoM Meso-scale Limited Area Prediction System (LAPS) model was used [14]. The Douglas sea state reported in Table 1 is based on the wave height. Figure 2 shows an example of the radar backscatter for HH polarization of run day 3 with a wind speed of 10.3 m/s and a wave height of 2.6 m. The data set was collected over a full 360 degree orbit of the scene and has been rotated so that upwind is at 0°. It is noteworthy that the imaged scenes contain waves driven from both wind and underlying swells. This is illustrated by the patterns observed in Fig. 2 which correspond to swell modulations. Although it was difficult to isolate the different wave and wind effects, the analysis performed helps to draw out interesting trends in the data.

In Fig. 3, significant wave heights, H_s, from the Ingara MGA data set are compared to those inferred from the classical Elfouhaily (Elf) spectral model [3] used in unlimited fetch conditions. As can be seen, the H_s values reported in the SCT04 campaign are much larger than those predicted by a fully-developed wind-sea surface, $H_s \simeq 0.025\ U^2$ where U is the wind speed at 10 m height, indicating the likely presence of large amplitude swell. On the contrary, the low H_s values observed for the MAST06 experiment are explained by data being subject to a daily wind cycle where the wind duration was constant for only a few hours in any given direction. This implies the seas during MAST06 were fully-developed only at very low wind speeds.

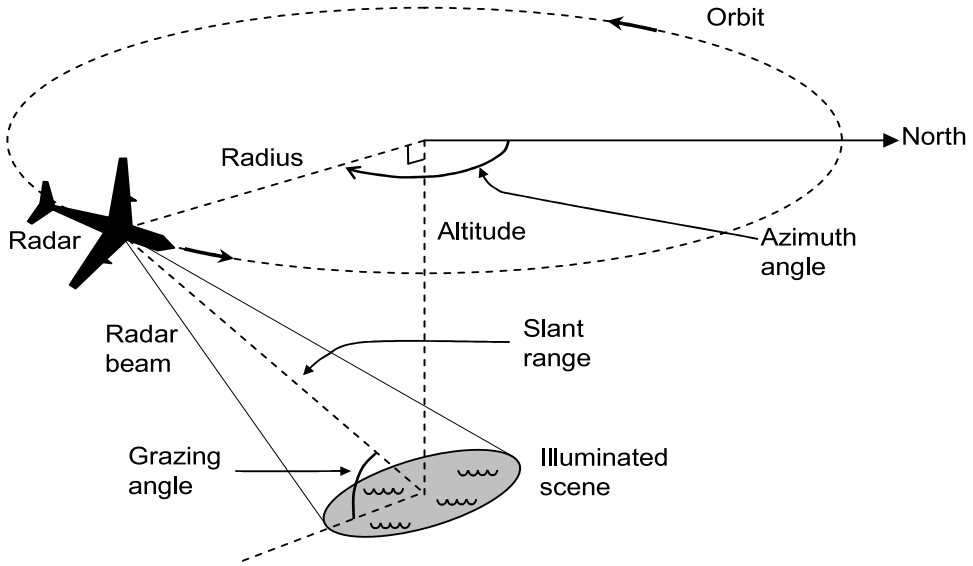

Figure 1: Circular spotlight mode collection geometry.

Table 1: Wind and wave ground truth for the Ingara MGA data. Run days 1-8 are from the SCT04 trial, while 9-12 are from MAST06. Douglas sea state is determined by the wave height.

Run day	Douglas sea state	Wind		Wave		
		Speed (m/s)	Direction (deg)	Height (m)	Direction (deg)	Period (s)
1	6	10.2	248	4.9	220	12.3
2	5	7.9	248	3.5	205	11.8
3	5	10.3	315	2.6	210	10.4
4	5	13.6	0	3.2	293	8.8
5	4-5	9.3	68	2.5	169	9.7
6	5	9.5	315	3.0	234	11.4
7	6	13.2	22	3.8	254	12.2
8	7	8.5	0	4.3	243	12.5
9	3	8.5	115	0.62	112	3.1
10	2	3.6	66	0.25	35	2.6
11	2	3.5	83	0.41	46	4.0
12	3	10.2	124	1.21	128	4.6

3.0 Data processing

To estimate the sea-clutter NRCS, a number of pre-processing steps were applied to the collected data. Firstly, the sampled signal was adjusted for motion compensation using both the inertial navigation unit and the global positioning system onboard the radar platform. The next steps included a correction for the variation in ground range resolution due to changes in grazing angle, removal of the elevation beampattern and polarimetric calibration using trihedral corner reflectors on the ground, assuming that calibration parameters are constant during the flight. Motion compensation affected the phase of the radar backscatter, while adjustment for the ground range resolution altered the NRCS. The calibration was validated by verifying the stability of the radar cross talk, channel imbalance and absolute gains for several hours before the flight.

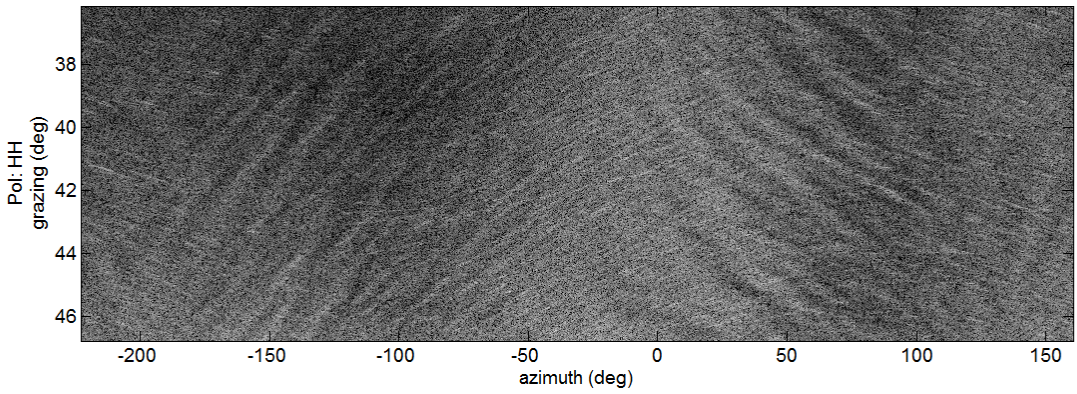

Figure 2: Example of Ingara HH sea-clutter data as a function of azimuth angle.

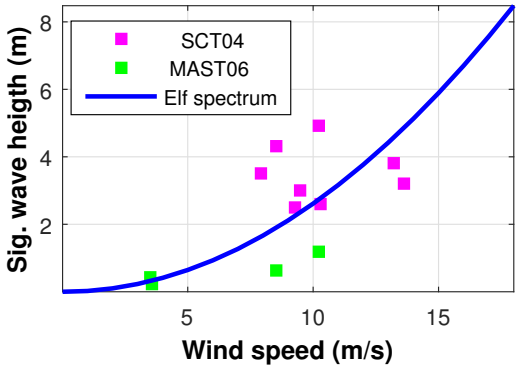

Figure 3: Significant wave height with respect to wind speed as derived from Elfouhaily spectrum and the measured environmental conditions during the Ingara MGA trials.

For the lower grazing angles and both HH and HV polarization channels, the SNR is low and an accurate denoising procedure is of primary importance for correct retrieval of the NRCS. In previous work [20], the mean instantaneous thermal noise power of the radar system was estimated by processing part of the collection where the transmitter was turned off. By assuming the sea-clutter and thermal noise are independent throughout the processing chain, a noise signal was then created in the backscatter coefficient domain with the same pre-processing steps applied as the clutter plus noise signal. It is important to note that the noise level is constant within the radar. However, the noise component of the radar return after pre-processing and calibration becomes slightly larger at lower grazing angles. A point-by-point denoising by subtracting this noise from the measured data is not always appropriate as it may result in non-physical negative intensities and if these are rejected in the estimate of the NRCS, there is the possibility of introducing an artificial bias. To overcome these limitations and obtain an estimate of the mean noise power in the low SNR regions, we have therefore proposed a new probabilistic denoising approach based on a maximum likelihood estimator (MLE).

We assume an additive white noise on the recorded NRCS, with mean and variance depending on the grazing angle but not the azimuthal direction. This last assumption is well supported by experimental evidence.

For the double purpose of estimating the ensemble-averaged NRCS and reducing the noise, we average data in bins of 5° in azimuth and 1° in grazing with each bin containing approximatively 10^6 samples. Then assuming that the statistical parameters describing both the noise and the NRCS do not vary appreciably in such a small angular domain, the ensemble-averaged NRCS at a given grazing angle can be written as a Fourier

series describing the azimuth variation with an additive Gaussian background noise:

$$\sigma_0^{\text{model}}(\phi_n) = \tilde{\sigma}_0(\phi_n) + b(\phi_n), \tag{3.0.1}$$

where ϕ_n is the azimuth angle relative to the wind direction, $b(\phi_n)$ is a realization of the mean noise and $\tilde{\sigma}_0(\phi_n)$ is the denoised NRCS described by the following model:

$$\tilde{\sigma}_0(\phi_n) = a_0 + \sum_{k=1}^{4} a_k \cos(k(\phi_n - \delta_k)). \tag{3.0.2}$$

Four harmonics have been found sufficient to reproduce the mean azimuthal variations in the NRCS (See [21]). Also, the NRCS extrema do not always coincide with the cardinal directions (up/down/cross wind) and are sometimes significantly shifted from their expected position. Therefore, we did not assume any a-priori symmetry with respect to wind direction and have introduced additional phase parameters, δ_n, in the cosine expansion. Note that the amplitude is an implicit function of polarization, grazing angle and sea state.

After averaging in each bin, the mean noise power can reasonably be described with a Gaussian distribution by virtue of the central limit theorem, even through it is known to follow an exponential distribution. Our analysis assumes that antenna and system noise are the dominant contributors to the noise estimates and that environment sources of noise variability with look direction (both azimuth and grazing angle) can be neglected. The antenna will contribute a grazing angle dependency in the system noise which has been estimated for the denoising process, while analysis has shown that the variation over azimuth is approximately constant and may be approximated with a constant mean, $\bar{b}$, and variance, σ_b^2. Also, since the denoised NRCS is deterministic, the overall NRCS model can be represented as a shifted normal distribution:

$$\sigma_0^{\text{model}}(\phi_n) \sim \mathcal{N}(\tilde{\sigma}_0(\phi_n) + \bar{b}, \sigma_b^2). \tag{3.0.3}$$

$$\mathcal{L} = -\frac{1}{2}\sum_{n=1}^{N_a} \log(2\pi\sigma_b^2) - \sum_{n=1}^{N_a} \frac{1}{2\sigma_b^2}[\sigma_0^{\text{data}}(\phi_n) - (\tilde{\sigma}_0(\phi_n) + \bar{b})]^2, \tag{3.0.4}$$

where N_a is the number of bins in azimuth. This can also be rewritten after substituting the NRCS model in (3.0.2):

$$\mathcal{L} = -\frac{1}{2}\sum_{n=1}^{N_a} \log(2\pi\sigma_b^2) - \left(\sum_{n=1}^{N_a} \frac{1}{2\sigma_b^2}[\sigma_0^{\text{data}}(\phi_n) - (a_0 + \sum_{k=1}^{4} a_k \cos(k(\phi_n - \delta_k)) + \bar{b})]^2 \right). \tag{3.0.5}$$

The parameters a_k and δ_k in the model NRCS can be obtained by maximization of the log-likelihood. This is performed by finding the set of values which cancel the partial derivatives $\frac{\partial \mathcal{L}}{\partial a_k}$ and $\frac{\partial \mathcal{L}}{\partial \delta_k}$. This leads to a linear system of size 9×9 for the 9 unknowns (a_0, a_k, δ_k), with matrix elements merely depending on the bin-averaged data $\sigma_0^{\text{data}}(\phi_k)$ and the mean noise power $\bar{b}$. Due to page constraints, the derivation is not reproduced here but is straightforward to obtain.

Figure 4 shows an example of the denoised NRCS, its comparison with the original data and the mean value of the azimuthal noise. As can be seen for low grazing angles where the SNR is low, the full dynamical range of the HH NRCS can only be seen after appropriate denoising.

To test the robustness of the estimation scheme, a validation procedure was performed by simulating the NRCS using the GO-SSA scattering model [22] introduced in Section 6.0 and then adding different levels of simulated noise. The root mean square error calculated between the noise-free simulated data and the estimated model is found to be significantly low and quite insensitive to the SNR (It remains of the order of 10^{-9} for an SNR as low as -30 dB). Another possible source of mismatch between model and data is the limited number of azimuthal harmonics in the model. This was verified by simulating a 10-harmonic NRCS and then reconstructing it with only 4 harmonics. The results were still found to be accurate and robust to the SNR.

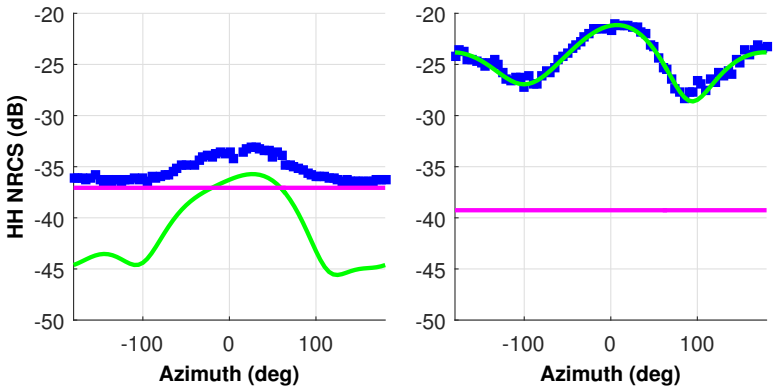

Figure 4: Raw (■) and denoised NRCS (green) for the HH polarization, run day 9 at grazing angles: 15° (left) and 45° (right). The mean noise estimate is shown in magenta. Note that the azimuth axis has been rotated so that 0° is upwind.

4.0 Angular variation of the NRCS

4.1 Grazing variations

The MLE based fitting and denoising procedure has been systematically applied to the different run days for all grazing angles. Figure 5 shows an example of the co-polarized NRCS (HH and VV) for run day 9 as a function of the grazing angle for different azimuthal directions: upwind, crosswind and downwind. The noise estimate exhibits a variation of up to 4 dB with grazing angle but only the mean value for this specific run day is superimposed on the plots, with the remaining solid lines corresponding to a third-order polynomial model that has been fitted to the NRCS.

In this figure, the upwind and downwind returns in VV are close, while the crosswind return is lower by about 7 dB. This is not the case in HH where the downwind and crosswind values are very close at the lowest grazing angles. In addition, the denoised NRCS in this region is up to 10 dB lower than the noise floor. We recall that the total collection across all grazing angles took approximately 90 minutes. Even though it seems reasonable to assume that the ocean surface conditions remain relatively stable over such short time intervals and that mean backscatter variations are for the most part related to the changing imaging geometry rather than changing ocean conditions, it is possible that this has caused some variations across grazing angles.

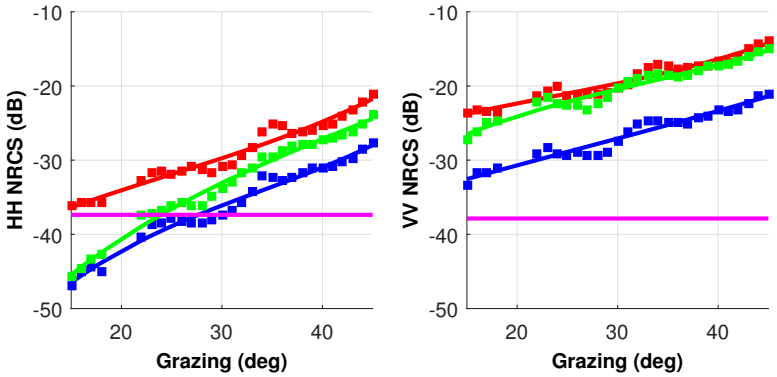

Figure 5: Variation of the NRCS with grazing angle for run day 9 for HH (left) and VV (right) polarizations. Azimuth directions: upwind (red), crosswind (blue) and downwind (green). Mean noise estimate is shown in magenta.

4.2 Azimuthal variations

We now investigate the azimuthal variation after the MLE based denoising. Figure 6 illustrates the azimuthal variations of the resulting co-polarized NRCS (VV and HH) for run day 9 (wind speed of 8.5 m/s) with various grazing angles. At moderate grazing angles we recover the commonly observed pattern of a sinusoidal variation with respect to the wind direction: a maximum in the upwind direction, a secondary maximum in the downwind direction and two minima in the crosswind directions. Note that the variations are sometimes asymmetric around the upwind direction which may be due to the occurrence of an extra swell system not aligned with the wind direction. This also can be linked to any potential wind measurement inaccuracy.

As the grazing angle is decreased in HH polarization, the angular distribution shifts progressively from two local maxima in the upwind/downwind direction to a unique and pronounced maximum in the upwind direction. The interpretation and physical modeling of this peculiar azimuthal behavior at low grazing angles are not easily established. To better characterize this observed behaviour, we have investigated the upwind/downwind asymmetry (UDA) and upwind/crosswind asymmetry (UCA). This is defined as the difference (in dB) of the NRCS level at the cardinal directions for the same grazing angle.

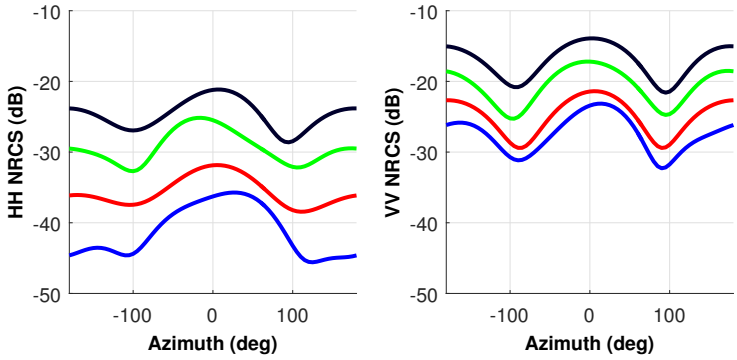

Figure 6: Azimuthal variation in HH (left) and VV (right) polarizations for run day 9 with nominal grazing angles of 16° (blue), 25° (red), 35° (green) and 45° (black). Note that the azimuth axis has been rotated so that 0° is upwind.

Observed values of the maximum UDA and UCA in the HH and VV polarizations, together with the grazing angle where these maxima occur have been reported. Note that values for the two crosswind directions ($\pm$90 degrees) have been averaged as they sometimes exhibit different levels of NRCS. This is seen in Fig. 6 and is likely due to the presence of a different wave system (swell) in the sea.

From these results, the UDA and UCA for both polarizations reach their maximum at a moderate grazing angle between 35° and 45°. This angle varies slightly with wind speed but no clear trend is observed. The maximum UDA in HH is about 2 dB higher than the VV counterpart, suggesting that the UDA is more pronounced at VV than HH polarization, while the maximum UCA is rather insensitive to polarization and wind speed ($\sim$ 7 dB at moderate to large winds speed between 8-14 m/s). Further conclusions are difficult to make for the UDA due to the small SNR and the strong data dispersion at lower grazing angles.

5.0 Relations between the different polarizations

To better understand the relationship between the different polarization channels, we now study the polarization ratio and difference as well as the azimuth variation of the cross polarized data.

5.1 Polarization ratio

The most commonly used quantity to relate the different polarization channels is the polarization ratio (PR),

$$PR = (\sigma^0_{VV})_{dB} - (\sigma^0_{HH})_{dB} \tag{5.0.6}$$

where the dB subscript indicates the result measured in decibels. An illustration of the variation with grazing angle is given in Fig. 7 for run days 9 (left) and 12 (right), where the PR is modelled using a third-order polynomial. Superimposed on this figure are the PR predicted by classical Bragg theory [23, eqns. 4.5-4.7], which is believed to be the dominant mechanism at medium grazing angles and low wind speed, as well as the PR inferred from the GOSSA model which offers a closer match to the data.

These results show the PR is a decreasing function with grazing and the Ingara MGA results are typically much lower than the (roughness independent) polarization ratio predicted by Bragg theory. The GO-SSA model is a closer match to the data and offers significant improvement to the PR prediction. However, it remains deficient in recovering the PR azimuthal variation (namely the upwind/downwind PR contrast and the maximum downwind PR). This discrepancy between data and models is especially true at 15° grazing, where a difference of up to 10 dB is observed. A strong sensitivity to the azimuthal direction is also observed, with a similar PR level observed in the up and crosswind directions, while the downwind PR is systematically higher. These trends are confirmed in Fig. 8 which shows the azimuthal variation of the PR. The results show a sharp maximum around the downwind direction and a secondary maximum around the upwind direction, which can allow removing the ambiguity usually encountered between the upwind and downwind directions.

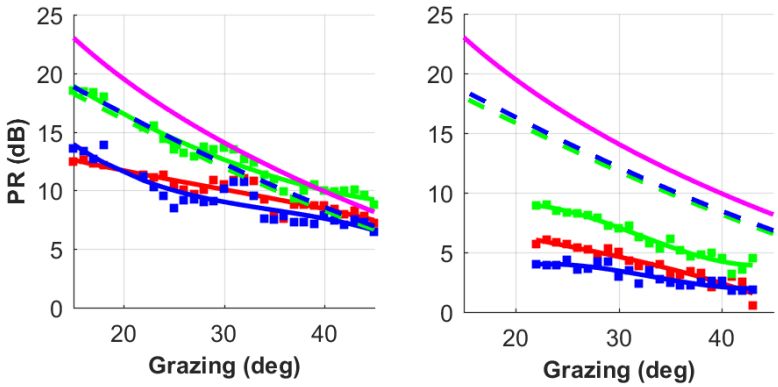

Figure 7: Polarization ratio versus grazing angle for run days 9 (left) and 12 (right). Azimuth direction: upwind (red), crosswind (blue) and downwind (green). The magenda solid line (–) corresponds to Bragg PR and the dashed lines (- -) and (- -) to GO-SSA upwind and crosswind PR respectively.

5.2 Polarization difference

Another useful parameter is the polarization difference (PD) of the two co-polarizations using a linear scale [24],

$$PD = (\sigma^0_{VV} - \sigma^0_{HH})_{dB}. \tag{5.0.7}$$

This parameter is also twice the polarized part, σ^0_{pol}, of the NRCS in its classical decomposition into a polarized and unpolarized part,

$$\begin{aligned} \sigma^0_{VV} &= \frac{1}{2}(\sigma^0_{VV} + \sigma^0_{HH}) + \frac{1}{2}(\sigma^0_{VV} - \sigma^0_{HH}) = \sigma^0_{unpol} + \sigma^0_{pol}, \\ \sigma^0_{HH} &= \frac{1}{2}(\sigma^0_{VV} + \sigma^0_{HH}) - \frac{1}{2}(\sigma^0_{VV} - \sigma^0_{HH}) = \sigma^0_{unpol} - \sigma^0_{pol}. \end{aligned} \tag{5.0.8}$$

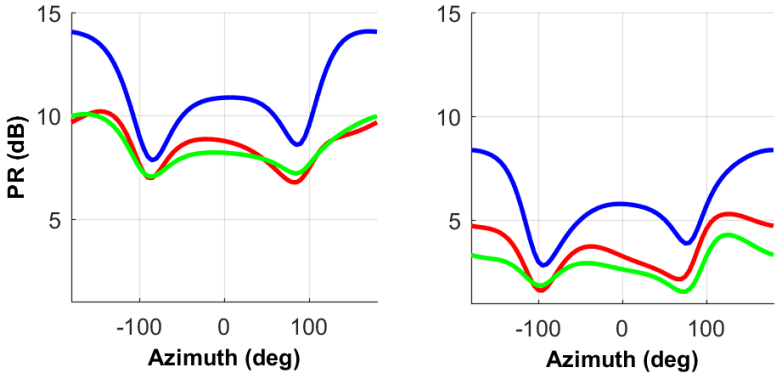

Figure 8: Polarization ratio versus azimuth angle for run days 9 (left) and 12 (right) at nominal grazing angles of 25°(blue), 37° (red) and 42° (green). Note that the azimuth axis has been rotated so that 0° is upwind.

It is well-known (see for example the Two-scale model or as a direct consequence of the universal weighted curvature approximation (WCA) [25, eq. 4.32]), that if one ignores the effect of the modulation by long waves, then the PD is proportional to the wave number spectrum taken at the Bragg frequency. It is therefore more sensitive to the small scale features of the sea surface, rather than the larger scales which are responsible for the unpolarized portion of the NRCS.

The azimuthal variations of the PD at various grazing angles have been studied. At lower grazing angles, the PD is typically dominated by the VV component which is much stronger than HH. However, at higher grazing angles where the VV and HH NRCS are of the same order of magnitude, the PD does not exhibit the UDA asymmetry seen with HH and VV polarized data. This seems to indicate that the UDA asymmetry is likely to be contained in the non-polarized part and presumably linked to the large rather than small scales of roughness. Another possibility is that breaking events, whose contribution is thought to be non-polarized, play a major role in the production of this asymmetry. This would explain why the UDA is stronger in HH than VV (the relative contribution of breaking being stronger in the former case).

5.3 Cross-polarized data

Similarly to the co-polarized data, we now study the azimuthal variation of the cross-polarized data. These data present an azimuthal modulation whose shape is akin to the VV-polarized data but which is remarkably less pronounced when compared to the co-polarized data in terms of asymmetry magnitudes. Since cross-polarized measurements are usually very close to the noise floor, these conclusions on azimuthal variations have been confirmed on the higher grazing angle HV data where the SNR is good enough to assign confidence to the results.

6.0 Model comparison

In this last section, we evaluate the performance of some currently available sea surface scattering models with the Ingara MGA sea clutter data set.

6.1 Choice of the spectral model

The co-polarized channels of the NRCS have been estimated with the improved Two-Scale model [22] referred to as ‘GO-SSA’ as it is based on a combination of the Geometrical Optics and the Small-Slope Approximation. In this calculation, both Elfouhaily and Bringer-Yuroskaya spectral models have been used for the

different wind speeds reported in Table 1. These spectral models have also been used to estimate the cross-polarized channels with using a recent simplified formulation [26] of the second-order small-slope approximation (SSA2), [27]. In this work, a numerically efficient and almost equivalent version of SSA2 was developed for the cross-polarized backscatter.

The results shown in Figs. 9-11 demonstrate that the recent BY spectral model brings significant improvement to the simulation of the NRCS. For the co-polarized channels, it is in close agreement with data for both upwind and crosswind directions. However, due to the elevated noise floor in the cross-polarized channel, a significant comparison can only be drawn in the upwind direction, where the agreement with the BY model is satisfactory.

The same conclusions are drawn from plots of azimuthal variation of Ingara data and associated model comparison. Although upwind/downwind as well as crosswind/crosswind asymmetries are not captured by centro-symmetric models (which results in azimuthal discrepancy between data and models especially when data exhibit strong asymmetries), the improvement brought by BY model is clearly shown in Fig. 10.

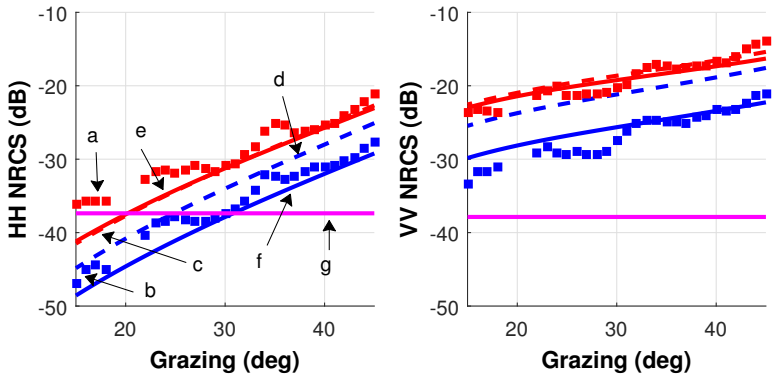

Figure 9: HH (left) and VV (right) NRCS from the Ingara MGA data for run day 9: a - upwind (■), b - crosswind (■). Superimposed is the simulated NRCS according to the GO-SSA model with Elfouhaily directional spectrum: c - upwind (- -), d - crosswind (- -) and Bringer-Yurovskaya model: e - upwind (–), f - crosswind (–). Mean noise estimate is shown in g - magenta.

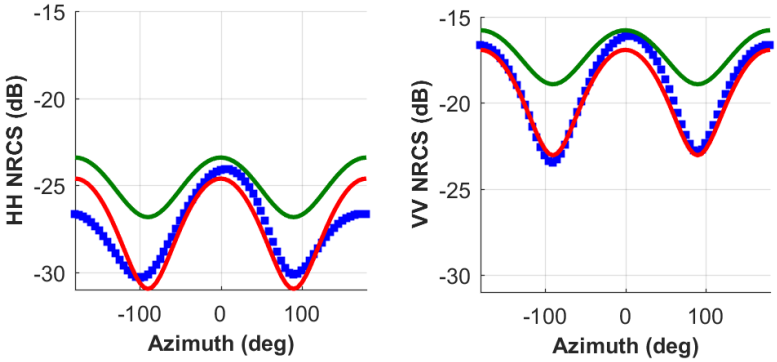

Figure 10: HH (left) and VV (right) azimuthal NRCS from the Ingara MGA data (■) for run day 9 at nominal grazing angle of 42°. Superimposed is the simulated NRCS according to the GO-SSA model with Elfouhaily directional spectrum (–) and Bringer-Yurovskaya model (–).

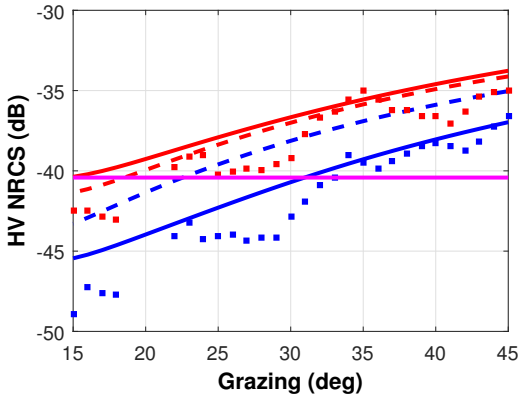

Figure 11: Same as Fig. 9 for the HV NRCS.

7.0 Conclusion

In this work, we have undertaken a thorough analysis of the geometric and polarimetric properties of the Ingara MGA sea clutter data set and introduced a novel probabilistic denoising procedure introduced for the low SNR regions. The data analysis has been complemented with a comparison of modern sea surface scattering models to evaluate their suitability for modelling real MGA sea clutter. Our main findings can be summarized as follows:

- The azimuthal behavior of the HH NRCS was confirmed at both medium and low grazing angles, with the latter demonstrating the vanishing of the secondary downwind maximum.
- The directional asymmetries were strongly polarization dependent and exhibited non-monotonic variations with respect to the grazing angle. The maximum UDA and UCA in the two co-polarizations lie at moderate grazing angles between about 35° and 45° with little sensitivity to wind speed. The HH NRCS favors the upwind/downwind asymmetry with a maximum UDA approximately 2 dB higher than the VV NRCS, while the maximum UCA did not exhibit clear variations with the polarization and wind speed, remaining around 7 dB at moderate to large wind speeds between 8-14 m/s.
- The polarization ratio was strongly dependent on the radar collection geometry and showed very different results at lower grazing angles than the value predicted from Bragg theory. The PR variation with respect to azimuth angle presented a sharp maximum in the downwind direction. Furthermore, we showed that the polarization difference between the two co-polarized NRCS channels has a much lower UDA than the HH and VV polarized NRCS, suggesting that the non-polarized NRCS (and therefore large scale wave structures or possibly breaking events) play a major role in the production of this asymmetry.
- For model assessment purposes, the GO-SSA model and a simplified version of the SSA2 model have been used to estimate the NRCS of the co- and cross-polarizations. A strong discrepancy between the model predictions and observations has been found in the case of the classical Elfouhaily directional spectrum. More consistent results were obtained by combining the recent spectral models of Bringer and Yurovskaya.

As perspective to this work, a further study is undertaken to improve our understanding of the physical mechanisms at the origine of the upwind/downwind asymmetry. This latter is commonly assigned to the modulation of the short waves riding on the long gravity waves: The ripples are more concentrated on the forward faces of the long waves compared to the rear faces, yieding corrections of the local incidence angle and thus changes in the average return signals. However, we believe that the UDA is not wholly explained by this modulation.

Numerous studies show that a non-polarized contribution must be taken into account, often linked to the presence of enhanced roughness features associated to breaking waves. An other plausible source of UDA is the deviation of the sea surface statistical properties from Gaussian. All these elements motivate a further study on the contribution of these different mechanisms to the sea surface asymmetries.

8.0 Acknowledgments

The Région Provence-Alpes-Côte d'Azur (PACA) and the ONERA are acknowledged for funding the PhD of Z. Guerraou. Special thanks go to the Defence Science and Technology Group for providing the Ingara MGA data set.

References

[1] T. Elfouhaily and C. A. Guérin. A critical survey of approximate scattering wave theories from random rough surfaces. *Waves in Random and Complex Media*, 14(4):1–40, 2004.

[2] G. J. Komen, L. Cavaleri, M. Donelan, K. Hasselmann, S. Hasselmann, and P. A. E. M. Janssen. *Dynamics and modelling of ocean waves*. Cambridge university press, 1996.

[3] T. Elfouhaily, B. Chapron, K. Katsaros, and D. Vandemark. A unified directional spectrum for long and short wind-driven waves. *J. Geophys. Res.*, 102(C7):15781–15796, July 1997.

[4] P. Janssen. *The interaction of ocean waves and wind*. Cambridge University Press, 2004.

[5] P.-Y. Le Traon, D. Antoine, A. Bentamy, H. Bonekamp, L. A. Breivik, B. Chapron, G. Corlett, G. Dibarboure, P. DiGiacomo, and C. Donlon et. al. Use of satellite observations for operational oceanography: recent achievements and future prospects. *Journal of Operational Oceanography*, 8(sup1):s12–s27, 2015.

[6] S. Tanelli, S. L. Durden, and E. Im. Simultaneous measurements of Ku-and Ka-band sea surface cross sections by an airborne radar. *IEEE Geoscience and Remote Sensing Letters*, 3(3):359–363, 2006.

[7] A. A. Mouche, B. Chapron, N. Reul, D. Hauser, and Y. Quilfen. Importance of the sea surface curvature to interpret the normalized radar cross section. *J. Geophys. Res.*, 112(C10):10002, 2007.

[8] N. Majurec, J. T. Johnson, S. Tanelli, and S. L. Durden. Comparison of model predictions with measurements of Ku- and Ka-band near-nadir normalized radar cross sections of the sea surface from the genesis and rapid intensification processes experiment. *IEEE Transactions on Geoscience and Remote Sensing*, 52(9):5320–5332, Sept 2014.

[9] G. Caudal, D. Hauser, R. Valentin, and C. Le Gac. KuROS: A new airborne Ku-band Doppler radar for observation of surfaces. *Journal of Atmospheric and Oceanic Technology*, 31(10):2223–2245, 2014.

[10] S. Angelliaume, V. Fabbro, G. Soriano, and C. A. Guerin. The go-ssa extended model for all-incidence sea clutter modeling. *Geoscience and Remote Sensing Symposium (IGARSS), 2014 IEEE International, Quebec City, QC, pp. 5017-5020*, 2014.

[11] A. G. Voronovich and V. U. Zavorotny. Theoretical model for scattering of radar signals in Ku-and C-bands from a rough sea surface with breaking waves. *Waves in Random Media*, 11(3):247–269, 2001.

[12] H. Johnsen, G. Engen, and G. Guitton. Sea-surface polarization ratio from Envisat ASAR AP data. *IEEE Transactions on Geoscience and Remote Sensing*, 46(11):3637–3646, 2008.

[13] A. Bringer, C.-A. Guérin, B. Chapron, and A. Mouche. Peakedness effects in near-nadir radar observations of the sea surface. *IEEE Transactions on Geoscience and Remote Sensing*, 50(9):3293–3301, 2012.

[14] L. Rosenberg and S. Watts. High grazing angle sea-clutter literature review. General Document DSTO-GD-0736, DSTO, 2013.

[15] F. E. Nathanson, J. P. Reilly, and M. N. Cohen. Radar design principles-signal processing and the environment. 91, 1991.

[16] F. T. Ulaby, R. K. Moore, and A. K. Fung. Microwave remote sensing: Active and passive. *Volume II: Radar Remote Sensing and Surface Scattering and Emission Theory*, 1982.

[17] D. J. Crisp, R. Kyprianou, L. Rosenberg, and N. J. Stacy. Modelling X-band sea clutter at moderate grazing angles. *IEEE International Radar Conference*, pages 596–601, 2008.

[18] M.M. Horst, F.B. Dyer, and M.T. Tuley. Radar sea clutter model. *Int. Conf. on Antennas and propagation, IEE Conf: Pub.169*, 1978.

[19] N. J. S. Stacy, D. Crisp, A. Goh, D. Badger, and M. Preiss. Polarimetric analysis of fine resolution X-band SAR sea clutter data. In *IEEE Geoscience and Remote Sensing Symposium*, volume 4, pages 2787–2790, 2005.

[20] L. Rosenberg, D. J. Crisp, and N. J. Stacy. Analysis of high grazing angle sea-cluter with the KK-distribution. Technical Report DSTO-TR-2915, DSTO, November 2013.

[21] C. Bourlier. Azimuthal harmonic coefficients of the microwave backscattering from a non-gaussian ocean surface with the first-order ssa model. *Geoscience and Remote Sensing, IEEE Transactions on , vol.42, no.11, pp.2600,2611*, Nov. 2004.

[22] G. Soriano and C. A. Guérin. A cutoff invariant two-scale model in electromagnetic scattering from sea surfaces. *IEEE Geoscience and Remote Sensing Letters*, 5(2):199–203, 2008.

[23] G. R. Valenzuela. Theories for the interaction of electromagnetic and oceanic waves- a review. *Boundary-Layer Meteorology*, 13(1):61–85, 1978.

[24] V.N. Kudryavtsev, B. Chapron, A.G. Myasoedov, F. Collard, and J.A. Johannessen. On dual co-polarized sar measurements of the ocean surface. *Geoscience and Remote Sensing Letters, IEEE , vol.10, no.4, pp.761,765*, July 2013.

[25] C.-A. Guérin, G. Soriano, and B. Chapron. The weighted curvature approximation in scattering from sea surfaces. *Waves in Random and Complex Media*, 20(3):364–384, 2010.

[26] C.-A. Guérin and J.-T. Johnson. A simplified formulation for rough surface cross-polarized backscattering under the second-order small-slope approximation. *IEEE Transactions on Geoscience and Remote Sensing*, 2015.

[27] A. Voronovich. Small-slope approximation for electromagnetic wave scattering at a rough interface of two dielectric half-spaces. *Waves in Random and Complex Media*, 4(3):337–367, 1994.